

(Anti)kaon condensation in strongly magnetized dense matter

Debraj Kundu,^{1,*} Vivek Baruah Thapa,^{1,†} and Monika Sinha^{1,‡}

¹*Indian Institute of Technology Jodhpur, Jodhpur 342037, India*

(Dated: October 27, 2022)

Recent observations of several massive pulsars, with masses near and above $2 M_{\odot}$, point towards the existence of matter at very high densities, compared to normal matter that we are familiar with in our terrestrial world. This leads to the possibility of appearance of exotic degrees of freedom other than nucleons inside the core of the neutrons stars (NS). Another significant property of NSs is the presence of high surface magnetic field, with highest range of the order of $\sim 10^{16}$ G. We study the properties of highly dense matter with the possibility of appearance of heavier strange and non-strange baryons, and kaons in presence of strong magnetic field. We find that the presence of a strong magnetic field stiffens the matter at high density, delaying the kaon appearance and, hence, increasing the maximum attainable mass of NS family.

I. INTRODUCTION

The state of matter inside neutron stars (NSs) is an unsolved mystery of modern science. Born from the remnants of a supernova explosion, a neutron star exhibits a range of densities inside its structure, the density of the core possibly being several times that of nuclear saturation density [1, 2]. Many recent astrophysical observations indicate that the possible lower limit of NS maximum mass is above $2 M_{\odot}$, viz. PSR J1614-2230 ($M = 1.97 \pm 0.04 M_{\odot}$) [3, 4], MSP J0740+6620 ($M = 2.14^{+0.20}_{-0.18} M_{\odot}$ with 95% credibility) [5], PSR J0348+0432 ($M = 2.01 \pm 0.04 M_{\odot}$) [6] and PSR J0952-0607 ($M = 2.35 \pm 0.17 M_{\odot}$) [7]. These findings strengthen the idea of existence of highly dense matter in the core of the NS. Thus, investigation of the matter inside NSs provides us with a unique opportunity to study matter under extreme conditions that cannot be emulated in our laboratories.

The gravitational pull inside the NS is balanced mostly by the Fermi degeneracy pressure of neutrons along with some amounts of protons and leptons (electrons and muons). In addition, the extreme matter density inside NSs can lead to energetically favourable conditions for exotic particles to appear. Hyperons are one such species of particles which might appear inside the NS if the baryon chemical potential becomes high enough. The possibility of their occurrence was first suggested in [8]. Another class of particle species that might make its appearance is Δ -resonances. Its appearance pushes the threshold for onset of hyperons to higher densities [9–11].

Similarly, another possible addition to the degrees of freedom can come from the appearance of meson condensates if the lepton chemical potential becomes high enough. However, for the lowest massive meson π , the repulsive s -wave pion-nucleon scattering potential increases the effective ground state mass of π -meson. Hence, the

possibility of π -meson's appearance is ruled out. On the other hand, for the next massive K -mesons, (anti)kaon ($\bar{K} \equiv K^-, \bar{K}^0$) mesons in the form of s -wave Bose condensates may appear due to the attractive nature of (anti)kaon optical potential. K^+ and K^0 kaons have repulsive optical potentials and their presence in nuclear matter increases their effective masses. Thus, the occurrence of K^+ and K^0 in NS matter is discouraged. The threshold density for the onset of \bar{K} is highly sensitive to its optical potential and whether or not hyperons are present [12]. The presence of \bar{K} in NS matter has been extensively studied [13–19].

As already mentioned, the verification of the theoretical models of highly dense matter can only be done with the observations from NSs. The astrophysical observable properties of NSs constructed by the dense matter models should be studied to constrain the models. For example, one should note that the appearance of hyperons tends to soften the equation of state (EoS) and, consequently, results in lowering of the maximum mass of NSs. Studies [9, 10] have indicated that the inclusion of Δ -resonances does not affect the implied maximum mass significantly, but it reduces the radius, and thereby, increases the compactness of the stars. The appearance of \bar{K} , similar to hyperons, softens the EoS and, thus, lowers the maximum mass of NSs.

The theoretical model of dense matter can be obtained from terrestrial laboratory data by extrapolating the nuclear matter properties at nuclear saturation density and can be further constrained from the recent mass-radius measurements of NSs, viz. the NICER mission observations give the mass-radius measurements of PSR J0030+0451 as $1.44^{+0.15}_{-0.14} M_{\odot}$, $13.02^{+1.24}_{-1.06}$ km [20] and $1.34^{+0.15}_{-0.16} M_{\odot}$, $12.71^{+1.14}_{-1.19}$ km [21], respectively. Another important constraint on highly dense matter inside NSs comes from the gravitational wave detection observations which provide us with the estimate of maximum limit of tidal deformability of the star made of highly dense matter.

Another salient feature of NSs is their strong surface magnetic field in the range $10^8 - 10^{16}$ G. A particular class of NSs which have ultra strong surface magnetic

* kundu.1@iitj.ac.in

† thapa.1@iitj.ac.in

‡ ms@iitj.ac.in

field of $10^{14} - 10^{16}$ G [22, 23] are called magnetars. The matter inside NS also experiences Pauli paramagnetism and Landau diamagnetism. Pauli paramagnetism is applicable for both charged and uncharged particles while the Landau diamagnetism affects only charged particles, being particularly strong for light particles like leptons. In our present work, we first note down the constraint on model parametrizations from the astrophysical observations of mass-radius measurements of many pulsars as well as tidal deformability from GW observations. Then with the constrained model we study the properties of dense matter and NSs with strong magnetic field.

Previous studies have been conducted on NS matter containing hyperons and Δ -resonances without (anti)kaon condensates [9, 10] and with (anti)kaon condensates [24]. The study without (anti)kaons was also extended to accommodate strong magnetic fields in [25]. Work has also been done on NS matter containing (anti)kaon condensates, but no hyperons or Δ -resonances, under the effect of strong magnetic fields [26, 27]. In this paper, we present the novel study of matter inside NS having a strong magnetic field (magnetar) containing hyperons, (anti)kaon condensates and Δ -resonances (as exotic degrees of freedom) in β -equilibrium. We have used the relativistic mean field (RMF) model to describe the interactions between the particles. As the soft matter with hyperons attains the lower limit of maximum mass with density dependent baryon-meson interactions, we use density dependent RMF (DD-RMF) model to study the effect of strong magnetic field on NS composed of matter with (anti)kaon condensates along with Δ resonances and hyperons.

In the next section (sec. II) we discuss the matter model under the effect of magnetic field. Then, in sec. III, we discuss the results with model parameters compatible with the the astrophysical observations. Section IV presents a brief summary of our work.

II. FORMALISM

A. DD-RMF Model

Here, we lay down the formulation for the DD-RMF model. We consider the NS matter to be composed of nucleons (n, p), leptons (e^-, μ^-), hyperons (Λ, Ξ, Σ), (anti)kaons ($\bar{K} \equiv K^-, \bar{K}^0$) and Δ -resonances ($\Delta^-, \Delta^0, \Delta^+, \Delta^{++}$). In this model, the strong interactions between the nucleons, hyperons, (anti)kaons and Δ -resonances are mediated by the following meson fields - isoscalar-scalar σ , isoscalar-vector ω^μ and isovector-vector ρ^μ . We have also considered the strange isoscalar-vector meson field ϕ^μ as a mediator of hyperon-hyperon and (anti)kaon-hyperon interactions. Throughout our work, we have used the natural units, $\hbar = c = G = 1$.

The total Lagrangian density is given by: [9, 13, 14, 26, 28–31]

$$\mathcal{L} = \mathcal{L}_m + \mathcal{L}_{em} \quad (1)$$

where \mathcal{L}_m and \mathcal{L}_{em} are the matter and the electromagnetic field contributions, respectively.

For the matter part of the Lagrangian density, We have

$$\begin{aligned} \mathcal{L}_m = & \sum_b \bar{\psi}_b (i\gamma_\mu D_\mu^b - m_b^*) \psi_b + \sum_d \bar{\psi}_{d\nu} (i\gamma_\mu D_\mu^d - m_d^*) \psi_{d\nu} \\ & + \sum_l \bar{\psi}_l (i\gamma_\mu D_\mu^l - m_l) \psi_l + D_\mu^{(\bar{K})} \bar{K} D_\mu^{(K)} K - m_K^{*2} \bar{K} K \\ & + \frac{1}{2} (\partial_\mu \sigma \partial^\mu \sigma - m_\sigma^2 \sigma^2) - \frac{1}{4} \omega_{\mu\nu} \omega^{\mu\nu} + \frac{1}{2} m_\omega^2 \omega_\mu \omega^\mu \\ & - \frac{1}{4} \rho_{\mu\nu} \cdot \rho^{\mu\nu} + \frac{1}{2} m_\rho^2 \rho_\mu \cdot \rho^\mu - \frac{1}{4} \phi_{\mu\nu} \phi^{\mu\nu} + \frac{1}{2} m_\phi^2 \phi_\mu \phi^\mu \end{aligned} \quad (2)$$

where $\psi_b, \psi_d^\nu, \bar{K}$ and ψ_l represent the fields of octet baryons, Δ -resonances, (anti)kaons and leptons, respectively. m_b, m_d, m_l and m_K stand for the masses of octet baryons, Δ -resonances, leptons and (anti)kaons, respectively. $\sigma, \omega_\mu, \rho_\mu$ and ϕ_μ are the meson fields with the masses $m_\sigma, m_\omega, m_\rho$ and m_ϕ , respectively. The covariant derivatives in Eqn.(2) are given by:

$$\begin{aligned} D_{\mu(j)} &= \partial_\mu + i g_{\omega j} \omega_\mu + i g_{\rho j} \tau_j \cdot \rho_\mu + i g_{\phi j} \phi_\mu + i e Q A_\mu \\ D_{\mu(l)} &= \partial_\mu + i e Q A_\mu \end{aligned} \quad (3)$$

with j representing the octet baryons (b), Δ -resonances (d) and (anti)kaons (\bar{K}), and (l) representing leptons. τ_j is the isospin operator for the ρ^μ meson fields. eQ is the charge of the particle with e being unit positive charge. We choose the direction of magnetic field as the z -axis with the field four-vector potential as $A^\mu \equiv (0, -yB, 0, 0)$, with B being the magnetic field magnitude. Under the effect of this magnetic field, the motion of the charged particles is Landau quantized in the plane perpendicular to the direction of field, the momentum in the perpendicular direction being $p_\perp = 2\nu e|Q|B$, where ν is the Landau level. Here, the baryon-meson coupling parameters are considered density dependent.

The gauge mesonic contributions in Eqn.(2) contain the field strength tensors:

$$\begin{aligned} \omega_{\mu\nu} &= \partial_\nu \omega_\mu - \partial_\mu \omega_\nu \\ \rho_{\mu\nu} &= \partial_\nu \rho_\mu - \partial_\mu \rho_\nu \\ \phi_{\mu\nu} &= \partial_\nu \phi_\mu - \partial_\mu \phi_\nu \end{aligned} \quad (4)$$

The effective masses of the baryons and (anti)kaons used in Eqn.(2) are given by:

$$\begin{aligned} m_b^* &= m_b - g_{\sigma b} \sigma \\ m_d^* &= m_d - g_{\sigma d} \sigma \\ m_K^* &= m_K - g_{\sigma K} \sigma \end{aligned} \quad (5)$$

$g_{\sigma j}$ in Eqn.(5) and $g_{\omega j}, g_{\rho j}, g_{\phi j}$ in Eqn.(3) are density dependent coupling parameters.

The electro-magnetic field part of the Lagrangian density in Eqn.(1) is given by:

$$\mathcal{L}_{em} = -\frac{1}{16\pi}F_{\mu\nu}F^{\mu\nu} \quad (6)$$

where $F_{\mu\nu}$ is the electro-magnetic field tensor.

In the relativistic mean field approximation, the meson fields acquire the following ground state expectation values:

$$\begin{aligned} \sigma &= \sum_b \frac{1}{m_\sigma^2} g_{\sigma b} n_b^s + \sum_d \frac{1}{m_\sigma^2} g_{\sigma d} n_d^s + \sum_{\bar{K}} \frac{1}{m_\sigma^2} g_{\sigma K} n_{\bar{K}}^s \\ \omega_0 &= \sum_b \frac{1}{m_\omega^2} g_{\omega b} n_b + \sum_d \frac{1}{m_\omega^2} g_{\omega d} n_d - \sum_{\bar{K}} \frac{1}{m_\omega^2} g_{\omega K} n_{\bar{K}} \\ \phi_0 &= \sum_b \frac{1}{m_\phi^2} g_{\phi b} n_b - \sum_{\bar{K}} \frac{1}{m_\phi^2} g_{\phi K} n_{\bar{K}} \\ \rho_{03} &= \sum_b \frac{1}{m_\rho^2} g_{\rho b} \tau_{b3} n_b + \sum_d \frac{1}{m_\rho^2} g_{\rho d} \tau_{d3} n_d \\ &\quad + \sum_{\bar{K}} \frac{1}{m_\rho^2} g_{\rho K} \tau_{\bar{K}3} n_{\bar{K}} \end{aligned} \quad (7)$$

where the scalar density $n_j^s = \langle \bar{\psi}\psi \rangle$ and the vector (baryon) number density $n_j = \langle \bar{\psi}\gamma^0\psi \rangle$.

The scalar density, baryon number density and the kinetic energy density of the uncharged baryons at the temperature $T = 0$ limit are given by:

$$\begin{aligned} n_u^s &= \frac{2J_u + 1}{2\pi^2} m_u^* \left[p_{F_u} E_{F_u} - m_u^{*2} \ln \left(\frac{p_{F_u} + E_{F_u}}{m_u^*} \right) \right] \\ n_u &= (2J_u + 1) \frac{p_{F_u}^3}{6\pi^2} \\ \varepsilon_u &= \frac{2J_u + 1}{2\pi^2} \left[p_{F_u} E_{F_u}^3 - \frac{m_u^{*2}}{8} \left(p_{F_u} E_{F_u} \right. \right. \\ &\quad \left. \left. + m_u^{*2} \ln \left(\frac{p_{F_u} + E_{F_u}}{m_u^*} \right) \right) \right] \end{aligned} \quad (8)$$

where J , p_F and E_F represent the spin, Fermi momentum and Fermi energy, respectively. Here the uncharged baryons are denoted by subscript u .

The scalar density, baryon number density and the kinetic energy density of the charged baryons at the temperature $T = 0$ limit are given by:

- For spin- 1/2 baryons:

$$n_c^s = \frac{e|Q|B}{2\pi^2} m_c^* \sum_{\nu=0}^{\nu_{max}} (2 - \delta_{\nu,0}) \ln \left(\frac{p_c(\nu) + E_{F_c}}{\sqrt{m_c^{*2} + 2\nu e|Q|B}} \right) \quad (9)$$

$$n_c = \frac{e|Q|B}{2\pi^2} \sum_{\nu=0}^{\nu_{max}} (2 - \delta_{\nu,0}) p_c(\nu) \quad (10)$$

$$\varepsilon_c = \frac{e|Q|B}{4\pi^2} \sum_{\nu=0}^{\nu_{max}} (2 - \delta_{\nu,0}) \left[p_c(\nu) E_{F_c} + \left(m_c^{*2} + 2\nu e|Q|B \right) \ln \left(\frac{p_c(\nu) + E_{F_c}}{\sqrt{m_c^{*2} + 2\nu e|Q|B}} \right) \right] \quad (11)$$

- For spin- 3/2 baryons:

$$n_c^s = \frac{e|Q|B}{2\pi^2} m_c^* \sum_{\nu=0}^{\nu_{max}} (4 - \delta_{\nu,1} - 2\delta_{\nu,0}) \ln \left(\frac{p_c(\nu) + E_{F_c}}{\sqrt{m_c^{*2} + 2\nu e|Q|B}} \right) \quad (12)$$

$$n_c = \frac{e|Q|B}{2\pi^2} \sum_{\nu=0}^{\nu_{max}} (4 - \delta_{\nu,1} - 2\delta_{\nu,0}) p_c(\nu) \quad (13)$$

$$\varepsilon_c = \frac{e|Q|B}{4\pi^2} \sum_{\nu=0}^{\nu_{max}} (4 - \delta_{\nu,1} - 2\delta_{\nu,0}) \left[p_c(\nu) E_{F_c} + \left(m_c^{*2} + 2\nu e|Q|B \right) \ln \left(\frac{p_c(\nu) + E_{F_c}}{\sqrt{m_c^{*2} + 2\nu e|Q|B}} \right) \right] \quad (14)$$

where $p(\nu) = \sqrt{p_F^2 - 2\nu eB}$. The charged baryons are denoted by subscript c . The maximum value of ν is given by:

$$\nu_{max} = \text{Int} \left(\frac{p_F^2}{2e|Q|B} \right) \quad (15)$$

The number density of (anti)kaon (\bar{K}) condensates is given by:

$$n_{K^-} = 2\sqrt{m_K^{*2} + |q_{K^-}|B} \bar{K}K \quad (16)$$

$$n_{\bar{K}^0} = 2m_K^* \bar{K}K \quad (17)$$

where $|q_{K^-}|$ is the charge of K^- .

In the case of leptons, the number density and kinetic energy density are given by:

$$n_l = \frac{e|Q|B}{2\pi^2} \sum_{\nu=0}^{\nu_{max}} (2 - \delta_{\nu,0}) p_l(\nu) \quad (18)$$

$$\varepsilon_l = \frac{e|Q|B}{4\pi^2} \sum_{\nu=0}^{\nu_{max}} (2 - \delta_{\nu,0}) \left[p_l(\nu) E_{F_l} + \left(m_l^2 + 2\nu e|Q|B \right) \ln \left(\frac{p_l(\nu) + E_{F_l}}{\sqrt{m_l^2 + 2\nu e|Q|B}} \right) \right] \quad (19)$$

The leptons are denoted by subscript l . Throughout Eqns.(8) - (19), we have

$$p_F = \sqrt{E_F^2 - m^{*2}} \quad (20)$$

The chemical potentials of octet baryons (b) with spin-1/2 and Δ -resonances (d) with spin- 3/2 are given by:

$$\mu_b = \sqrt{p_{F_b}^2 + m_b^{*2}} + g_{\omega b}\omega_0 + g_{\rho b}\tau_{b3}\rho_{03} + g_{\phi b}\phi_0 + \Sigma^r \quad (21)$$

$$\mu_d = \sqrt{p_{F_d}^2 + m_d^{*2}} + g_{\omega d}\omega_0 + g_{\rho d}\tau_{d3}\rho_{03} + \Sigma^r \quad (22)$$

Σ^r represents the self-energy re-arrangement term and is given by :

$$\begin{aligned} \Sigma^r = & \sum_b \left[\frac{\partial g_{\omega b}}{\partial n} \omega_0 n_b - \frac{\partial g_{\sigma b}}{\partial n} \sigma n_b^s + \frac{\partial g_{\rho b}}{\partial n} \rho_{03} \tau_{b3} n_b \right. \\ & \left. + \frac{\partial g_{\phi b}}{\partial n} \phi_0 n_b \right] + \sum_d \left[\frac{\partial g_{\omega d}}{\partial n} \omega_0 n_d - \frac{\partial g_{\sigma d}}{\partial n} \sigma n_d^s \right. \\ & \left. + \frac{\partial g_{\rho d}}{\partial n} \rho_{03} \tau_{d3} n_d \right] \quad (23) \end{aligned}$$

where $n = \sum_b n_b + \sum_d n_d$ is the total vector (baryon) number density. Σ^r is required in case of density dependent coupling models in order to maintain thermodynamic consistency [17]. The chemical potential of s-wave condensates of (anti)kaons is given by:

$$\mu_{K^-} = \sqrt{m_L^{*2} + |q_{K^-}|B} - g_{\omega K}\omega_0 - \frac{1}{2}g_{\rho K}\rho_{03} + g_{\phi K}\phi_0 \quad (24)$$

$$\mu_{\bar{K}^0} = m_K^* - g_{\omega K}\omega_0 + \frac{1}{2}g_{\rho K}\rho_{03} + g_{\phi K}\phi_0 \quad (25)$$

Threshold condition for the onset of the i^{th} baryon is given by:

$$\mu_i = \mu_n - q_i \mu_e \quad (26)$$

with $\mu_e = \mu_n - \mu_p$ being the electron chemical potential. q_i refers to the charge of the i^{th} baryon.

The threshold condition for the appearance of (anti)kaons is given by:

$$\mu_{K^-} = \mu_e = \mu_n - \mu_p \quad (27)$$

$$\mu_{\bar{K}^0} = 0 \quad (28)$$

where μ_{K^-} and $\mu_{\bar{K}^0}$ are the chemical potentials of K^- and \bar{K}^0 , respectively. Muons (μ^-) appear when the chemical potential of electrons reaches the rest mass of muons [$\mu_e = m_\mu$].

The matter inside NS is electrically neutral, with the charge neutrality condition given by:

$$\sum_b q_b n_b + \sum_d q_d n_d - n_e - n_\mu - n_{K^-} = 0 \quad (29)$$

The total energy density of the nuclear matter is given by:

$$\begin{aligned} \varepsilon = & \sum_b \varepsilon_b + \sum_d \varepsilon_d + \sum_l \varepsilon_l + \frac{1}{2}m_\sigma^2 \sigma^2 + \frac{1}{2}m_\omega^2 \omega_0^2 \\ & + \frac{1}{2}m_\rho^2 \rho_{03}^2 + \frac{1}{2}m_\phi \phi_0^2 + \varepsilon_{\bar{K}} \quad (30) \end{aligned}$$

where $\varepsilon_{\bar{K}}$ is the kaonic contribution to the total energy density and is given by:

$$\varepsilon_{\bar{K}} = m_K^* (n_{K^-} + n_{\bar{K}^0}) \quad (31)$$

From the Gibbs-Duhem relation, we get the matter pressure as:

$$P = \sum_b \mu_b n_b + \sum_d \mu_d n_d + \sum_l \mu_l n_l + n \Sigma^r - \varepsilon \quad (32)$$

(Anti)kaons, being s-wave condensates, do not contribute explicitly to the matter pressure. Σ^r contributes explicitly only to the matter pressure.

B. Star structure

The solution for the Einstein's equations for general relativity for a static and spherically symmetric star gives us the Tolman-Oppenheimer-Volkoff (TOV) equations. These equations are then numerically solved for a particular EoS to obtain the mass-radius relationship of the NS. The TOV equations are as follows [1]:

$$\begin{aligned} \frac{dP(r)}{dr} &= - \frac{[P(r) + \varepsilon(r)][M(r) + 4\pi r^3 P(r)]}{r[r - 2M(r)]} \\ \frac{dM(r)}{dr} &= 4\pi r^2 \varepsilon(r) \quad (33) \end{aligned}$$

where $M(r)$ is the gravitational mass included within radius r . The TOV equations are solved with the boundary conditions $M(0) = 0$ and $P(R) = 0$, where R is the radius of the NS. The presence of strong magnetic field, however, distorts the spherical symmetry of the star structure. The most general coupled set of equations determining the spherically symmetric star structure, as derived by Bowers and Liang, is given as [32]:

$$\begin{aligned} \frac{dM(r)}{dr} &= 4\pi r^2 \varepsilon \\ \frac{d\Phi(r)}{dr} &= \left(1 - \frac{2M}{r}\right)^{-1} \left(\frac{M}{r^2} + 4\pi P_r r\right) \\ \frac{dP_r(r)}{dr} &= -(\varepsilon + P_r) \frac{d\Phi}{dr} + \frac{2}{r}(P_\perp - P_r) \quad (34) \end{aligned}$$

where P_r and P_\perp are the radial and tangential pressure components, respectively, and Φ is the Newtonian gravitational potential at the Newtonian limit. The most

TABLE I: Table for nuclear saturation properties for the three parametrizations- DD-ME2, DD-2 and DD-MEX.

Parametrization	n_0 (fm^{-3})	E/A (MeV)	K_0 (MeV)	E_{sym} (MeV)	L_{sym} (MeV)	m_N^*/m_N	m_σ (MeV)	m_N (MeV)
DD-ME2	0.152	-16.14	250.89	32.30	51.253	0.572	550.124	938.90
DD-2	0.149065	-16.02	242.70	32.73	54.966	0.5625	546.2124	939.56
DD-MEX	0.152	-16.097	267.059	32.269	49.576	0.556	547.3327	939.00

TABLE II: Table for parameter values for DD-ME2, DD-2 and DD-MEX parametrizations. The masses of ω , ρ and ϕ mesons are 783 MeV, 763 MeV and 1019.45 MeV, respectively, and they are same for all the three parametrizations.

Parametrization	Meson(i)	a_i	b_i	c_i	d_i	g_{iN}
DD-ME2	σ	1.3881	1.0943	1.7057	0.4421	10.5396
	ω	1.3892	0.9240	1.4620	0.4775	13.0189
	ρ	0.5647				7.3672
DD-2	σ	1.3576	0.6344	1.0053	0.5758	10.6866
	ω	1.3697	0.4964	0.8177	0.6384	13.3423
	ρ	0.5189				7.2538
DD-MEX	σ	1.3970	1.3349	2.0671	0.4016	10.7067
	ω	1.3926	1.0919	1.6059	0.4556	13.3388
	ρ	0.6202				7.2380

general energy-momentum tensor, considering spherical symmetry, is :

$$T^{\mu\nu} = \text{diag}(\varepsilon, P_r, P_\perp, P_\perp) \quad (35)$$

However, following the same argument given in [33], $T^{\theta\theta} \neq T^{\phi\phi}$ (Eqns.(23d) & (23e) in [34]) for the case of the electromagnetic energy-momentum tensor. This is in contradiction to the spherical symmetry assumption in Eqn.(35). Also, the last term in Eqn.(34) diverges at the origin since $\lim_{r \rightarrow 0}(T^{rr} - T^{\theta\theta}) \neq 0$. Therefore, we see that spherically symmetric solutions cannot exactly describe the star structure in the presence of magnetic field. Although Eqn.(33) provides a good approximation of the M-R relation of magnetized NS [33], for central magnetic fields close to 10^{18} G the deformity becomes too large for Eqn.(33) to be used [35]. Thus, we refrain from using the spherically symmetric TOV equations for magnetic field strengths of $> 10^{17}$ G.

III. RESULTS AND DISCUSSION

A. Parametrizations

In this DD-RMF model, the density dependant nature of the meson-nucleon coupling constants for σ and ω mesons is given by:

$$g_{iN}(n) = g_{iN}(n_0)f_i(x), \quad i = \sigma, \omega \quad (36)$$

where n and n_0 are the total baryon number density and the nuclear saturation density, respectively. N refers to

nucleons. The variable $x = n/n_0$. $f_i(x)$ is defined as:

$$f_i(x) = a_i \frac{1 + b_i(x + d_i)^2}{1 + c_i(x + d_i)^2}. \quad (37)$$

The meson-nucleon coupling constant for ρ meson is given by:

$$g_{\rho N} = g_{\rho N}(n_0)e^{-a_\rho(x-1)}. \quad (38)$$

The ϕ meson does not couple with nucleons and, thus, $g_{\phi N} = 0$. We take $m_\omega = 783$, $m_\rho = 763$ and $m_\phi = 1019.45$ MeV.

For the calculation of the scalar meson-hyperon coupling constants, we consider the optical potentials of Λ , Ξ and Σ to be $U_\Lambda = -30$ MeV, $U_\Xi = -14$ MeV and $U_\Sigma = +30$ MeV, respectively [25]. Σ hyperons, having a repulsive optical potential, do not appear in the range of densities considered in our work.

In case of the vector meson-hyperon density dependent vector coupling constants, we employ SU(6) [36] symmetry and get the following relations:

$$\begin{aligned} \frac{1}{2}g_{\omega\Lambda} &= g_{\omega\Xi} = \frac{1}{2}g_{\omega\Sigma} = \frac{1}{3}g_{\omega N} \\ 2g_{\phi\Sigma} &= 2g_{\phi\Lambda} = g_{\phi\Xi} = -\frac{2\sqrt{2}}{3}g_{\omega N} \\ \frac{1}{2}g_{\rho\Sigma} &= g_{\rho\Xi} = g_{\rho N} \\ g_{\rho\Lambda} &= 0 \end{aligned} \quad (39)$$

For the scalar meson- Δ coupling constants, we fix the Δ -potential to $V_\Delta = \frac{4}{3}V_N$, which gives $R_{\sigma\Delta} =$

$g_{\sigma\Delta}/g_{\sigma N} = 1.16$. V_N stands for the nucleon potential. For Δ -resonances, the vector coupling constants are given by [37]:

$$g_{\omega\Delta} = 1.1g_{\omega N}, \quad g_{\rho\Delta} = g_{\rho N}.$$

ϕ meson does not couple with Δ -resonances and $g_{\phi\Delta} = 0$.

The calculation for the scalar meson-(anti)kaon coupling constants is explained in [19]. Several works [19] have provided the K^- optical potential ($U_{\bar{K}}$) in the $-200 \leq U_{\bar{K}} \leq -40$ MeV. In this work, we have $U_{\bar{K}} = -130$ MeV. The determination of vector (anti)kaon coupling constants is given in [12, 43]. They are density independent and are given by the relation

$$g_{\omega K} = \frac{1}{3}g_{\omega N}, \quad g_{\rho K} = g_{\rho N}, \quad g_{\phi K} = 4.27$$

In this work, we use three different density dependent parametrizations: DD-ME2, DD2 and DD-MEX. The three parametrizations are framed to reproduce the nuclear matter properties at n_0 . The nuclear saturation properties as well as the masses of nucleons and σ mesons for the three parametrizations are shown in Table I. In the table, E/A , K_0 , E_{sym} , L_{sym} , m_N , m_N^* and m_σ stand for binding energy per nucleon, compression modulus, symmetry energy coefficient, slope parameter of E_{sym} , mass of nucleons, effective mass of nucleons and mass of σ mesons, respectively. All the properties in Table I are evaluated at nuclear saturation density (n_0). The values of the coefficients in Eqns.(37) and (38) for the parametrizations DD-ME2 [44], DD2 [45] and DD-MEX [46] are given in Table II. \bar{K} condensates can appear via both first order and second order phase transitions. However, we note that with the discussed parametrizations only the second order phase transition occurs [19].

With these three parametrizations we note the star structure, ignoring the effect of magnetic field, from the mass-radius relation as shown in Fig. 1. From the figure, it is evident that the NSs composed of matter including hyperons, Δ resonances and (anti)kaon condensates satisfy the so far obtained astrophysical constraints on mass-radius relation for DD-MEX and DD-ME2 parametrizations. Even though it does not satisfy the most recent observation PSR J0952-0607, we still keep the DD-ME2 parametrization because it satisfies all the other observational constraints. Along with this, these two parametrizations also obey the maximum limit of mutual tidal deformability obtained from gravitational wave observations of binary NS merger event GW170817, which is evident from the Fig. 2. So, in our present study of the effect of magnetic field on the NS composed of matter containing hyperons, Δ -resonances and (anti)kaon condensates, we choose these two parametrizations which are compatible with astrophysical observations.

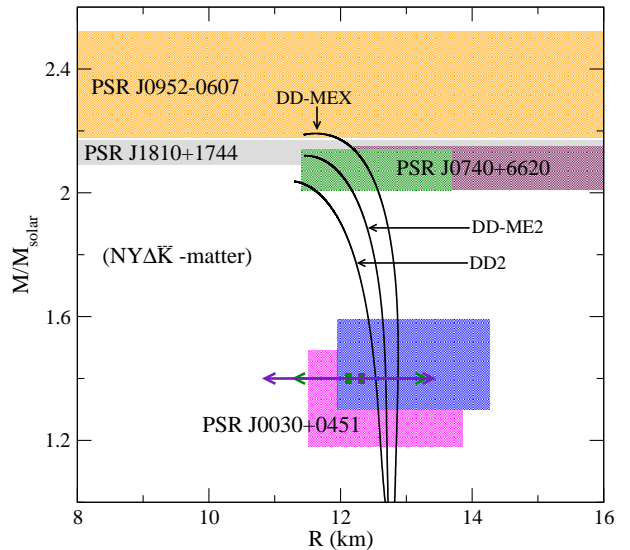


FIG. 1: Mass-radius relationship of NS for the matter composition $N\bar{K}Y\Delta$ for the parametrizations DD-ME2, DD-2 and DD-MEX. The shaded regions illustrate the observational constraints from PSR J0740+6620 [47, 48], PSR J1810+1744 [49], PSR J0030+0451 [50–53] and PSR J0952-0607 [7].

B. Magnetic Field Profile

We model the magnetic field inside NS by adopting a magnetic field profile which is consistent with the Einstein-Maxwell field equations. One such magnetic field profile has been obtained by finding the solutions of the Einstein-Maxwell field equations with magnetostatic equilibrium for EoS from several nuclear models and then taking a polynomial fit of the monopolar part of the norm of the magnetic field profiles obtained. This is the universal profile given by [33]

$$B(x) = B_m(1 - 1.6x^2 - x^4 + 4.2x^6 - 2.4x^8) \quad (42)$$

where $x \equiv r/r_{mean}$, r being the radial distance, r_{mean} is the mean radius of the star and B_m is the field strength at the centre of the star. This profile, however, is for a star with an approximate monopolar magnetic structure and does not incorporate the dipolar structure.

Another such profile, obtained by taking a quadratic fit of the solutions of Einstein-Maxwell field equations assuming a poloidal magnetic field for EoS from three different nuclear models and two different values of magnetic dipole moment, is given by [56, 57]:

$$B(\mu_B) = \frac{(a + b\mu_B + c\mu_B^2)}{B_c} \mu \quad (43)$$

where μ_B is the baryon chemical potential and μ is the dipole magnetic moment of the NS. μ_B and μ are in units of MeV and Am^2 , respectively, to get $B(\mu_B)$ in units of gauss (G). $B_c = 4.414 \times 10^{13}$ G is the critical field of

electron. The values of the coefficients a , b , c for a star of mass $2.2M_{\odot}$ are as follows:

$$\begin{aligned} a &= -0.769 G^2/(Am)^2 \\ b &= 1.2 \times 10^{-3} G^2/(Am^2 MeV), \\ c &= -3.46 \times 10^{-7} G^2/(Am^2 MeV^2) \end{aligned}$$

This magnetic field profile, being a function of baryon chemical potential, also avoids discontinuities in the field during phase transitions. Hence, we choose this profile in our following calculations. Here, we consider two values of the dipole magnetic moment, $\mu = 2 \times 10^{31} Am^2$ and $\mu = 1.5 \times 10^{32} Am^2$, which give central magnetic fields of around 1.2×10^{17} and $0.9 \times 10^{18} G$, respectively, and surface magnetic fields of around $2.5 \times 10^{16} G$ and $2 \times 10^{17} G$, respectively. The magnetic field profiles for each case are shown in Fig. 3.

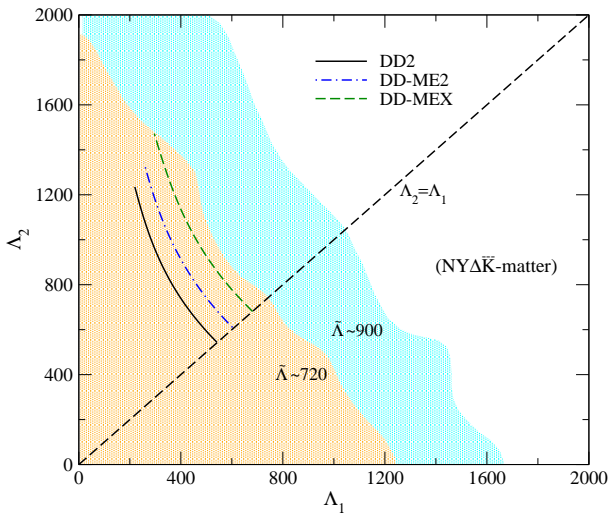


FIG. 2: Plot for the tidal deformabilities Λ_1 and Λ_2 for the matter composition $N\bar{K}Y\Delta$ and considering a fixed chirp mass, $\mathcal{M} = 1.188M_{\odot}$. The Λ_1 and Λ_2 correspond to the stars of masses M_1 and M_2 , respectively, of the binary system observed in GW170817 event. The shaded regions represent $\tilde{\Lambda} \sim 900$ (TaylorF2) and $\tilde{\Lambda} \sim 720$ (PhenomPNRT) upper bounds at 90% confidence level [54, 55].

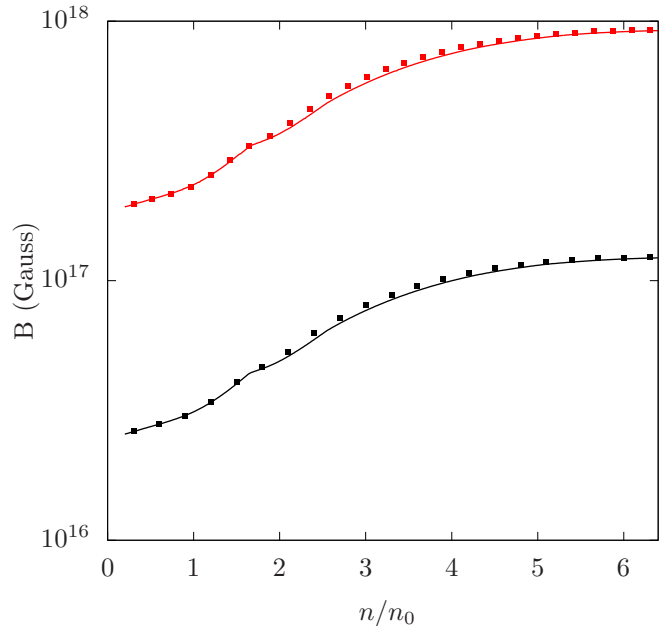


FIG. 3: The variation of magnetic field with the normalized number density n/n_0 corresponding to the magnetic field profile given by eq. (43). The upper curves are for $\mu = 1.5 \times 10^{32} Am^2$ and the lower curves are for $\mu = 2 \times 10^{31} Am^2$. The solid lines represent DD-ME2 parametrization while the dotted lines represent DD-MEX parametrization.

C. Matter and star with magnetic field

The particle fraction profiles for $NY\bar{K}\Delta$ are illustrated in Fig. 4 for the two parametrizations, both with and without magnetic field. The particle population at all densities satisfies the two conditions- charge neutrality and baryon number conservation. As can be inferred from the figure, at the initial densities, the charge neutrality is maintained by protons (p) and leptons- electrons (e^-) and muons (μ^-). The e^- and μ^- populations clearly decreases from the onset of the negative Δ -resonance (Δ^-) till they eventually disappear or become insignificantly sparse. This is because Δ^- is energetically more favourable than the leptons and thus take their place in maintaining charge neutrality. The onset of Ξ^- further contributes to the decrease in e^- population. The Δ^- population, however, starts to decrease with the onset of Ξ^- and decreases more heavily with the onset of K^- . At the extreme higher end of the density range, the negative charges are provided by K^- , Δ^- and Ξ^- while the positive charges are provided by p , Δ^+ and Δ^{++} , in a way such that charge neutrality remains intact. However, we note that Δ^{++} only appears in the case for DD-MEX parametrization and is absent in the case of DD-ME2.

The effect of magnetic field on the particle population can be better appreciated by looking at Fig. 5 and Fig.

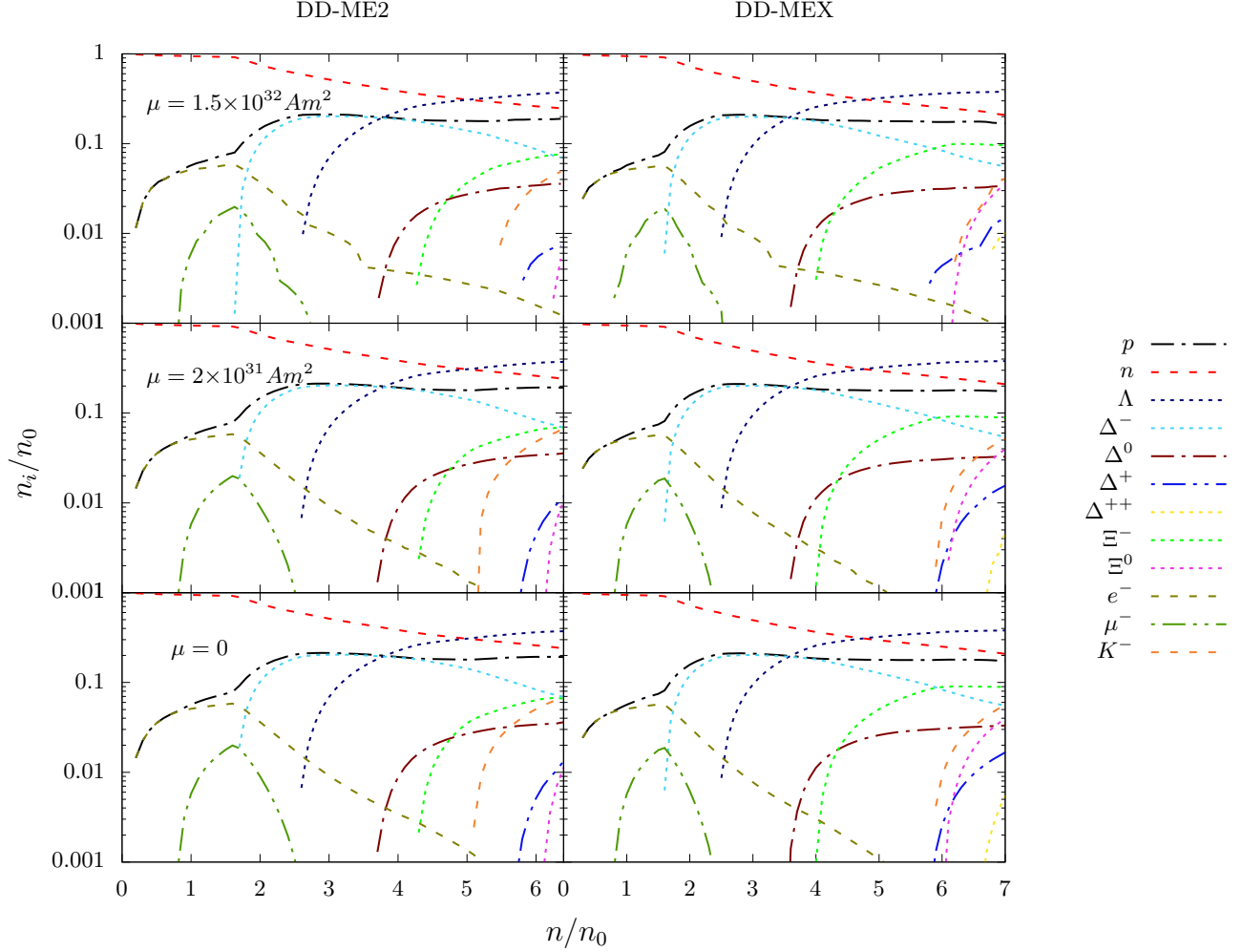


FIG. 4: Variation of particle number density normalized to the nuclear saturation density (n_i/n_0) with the total number density normalized to n_0 (n/n_0). Top panel: in the presence of magnetic field with $\mu = 1.5 \times 10^{32} \text{ Am}^2$, middle panel: in the presence of magnetic field with $\mu = 2 \times 10^{31} \text{ Am}^2$ and bottom panel: in the absence of magnetic field. Left panel: for DD-ME2 and right panel: DD-MEX parametrization.

TABLE III: Threshold densities of various particles. The particle μ^- extinguishes at 2.77 and 2.59 for DD-ME2 and DD-MEX, respectively, for B field with $\mu = 2 \times 10^{31} \text{ Am}^2$, and the particle μ^- extinguishes at 2.79 and 2.62 for DD-ME2 and DD-MEX, respectively, for B field with $\mu = 1.5 \times 10^{32} \text{ Am}^2$. Without magnetic field, the particle μ^- extinguishes at 2.77 and 2.58 for DD-ME2 and DD-MEX, respectively.

	$\mu = 1.5 \times 10^{32} \text{ Am}^2$		$\mu = 2 \times 10^{31} \text{ Am}^2$		Without B field	
	DD-ME2	DD-MEX	DD-ME2	DD-MEX	DD-ME2	DD-MEX
μ^-	0.75	0.75	0.75	0.75	0.75	0.75
Λ	2.53	2.42	2.53	2.42	2.53	2.42
Δ^-	1.63	1.58	1.63	1.58	1.63	1.58
Δ^0	3.61	3.50	3.61	3.50	3.61	3.50
K^-	5.37	6.11	5.11	5.87	5.07	5.82
Δ^+	5.75	5.72	5.64	5.71	5.62	5.70
Δ^{++}		6.70		6.57		6.55
Ξ^-	4.21	3.94	4.24	3.97	4.24	3.97
Ξ^0	6.16	6.08	6.08	6.00	6.06	5.99

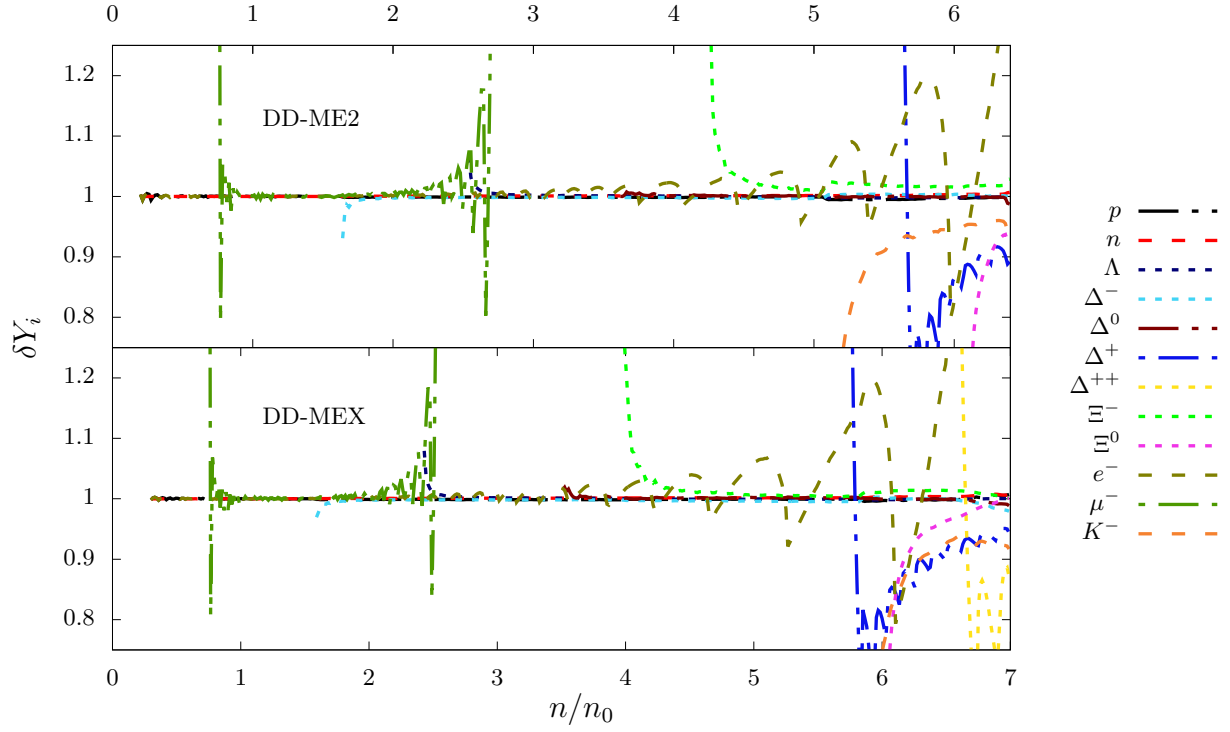


FIG. 5: Variation of $\delta Y_i = n_i(B)/n_i(0)$ with the total number density normalized to n_0 (n_i/n_0) for the star dipole moment $\mu = 2 \times 10^{31} Am^2$. Upper panel: DD-ME2 parametrization and lower panel: DD-MEX parametrization.

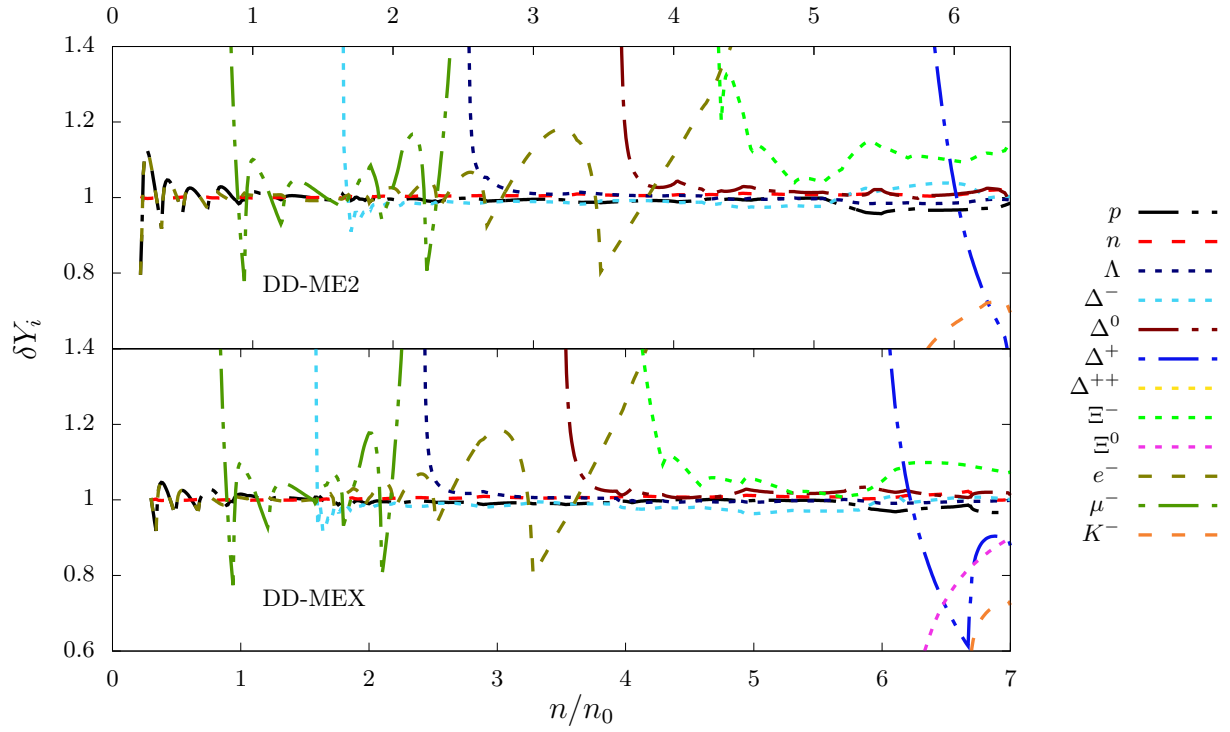


FIG. 6: Variation of $\delta Y_i = n_i(B)/n_i(0)$ with the total number density normalized to n_0 (n_i/n_0) for the star dipole moment $\mu = 1.5 \times 10^{32} Am^2$. Upper panel: DD-ME2 parametrization and lower panel: DD-MEX parametrization.

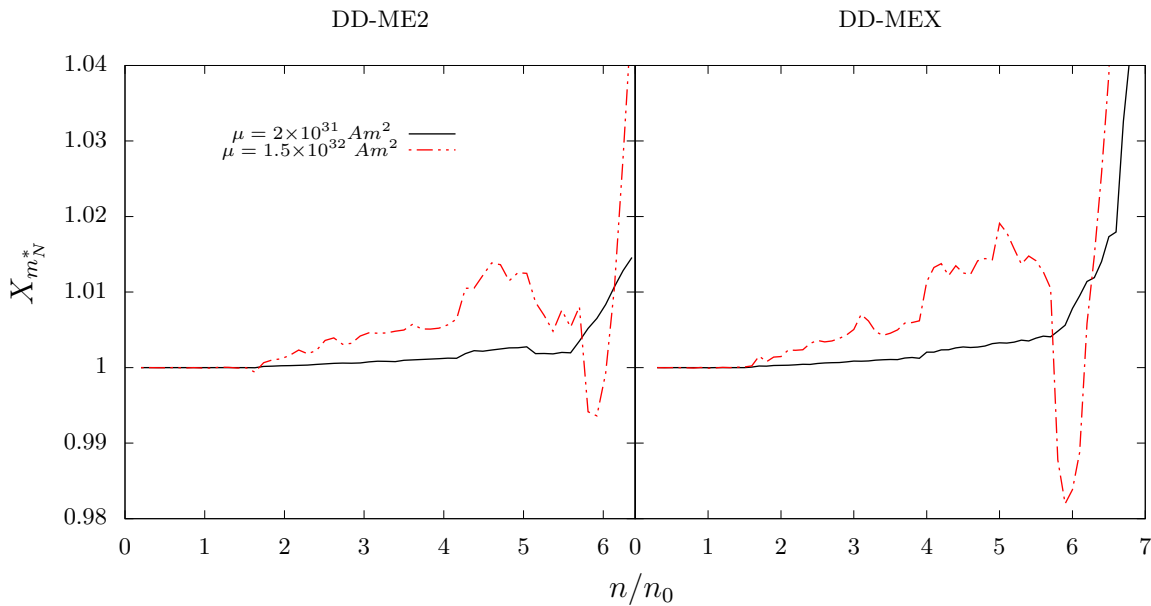


FIG. 7: Plot for the ratio $X_{m_N^*} \equiv m_N^*(B)/m_N^*(0)$ of the effective Dirac mass of nucleons in the presence of magnetic field to its value in the absence of magnetic field as function of total number density normalized to n_0 (n/n_0) for the star dipole moments $\mu = 2 \times 10^{31} Am^2$ and $\mu = 1.5 \times 10^{32} Am^2$. The plots are given for the matter matter composition $N\bar{K}Y\Delta$ and for the two parametrizations: DD-ME2 (left panel) and DD-MEX (right panel).

6. They show the ratio $\delta Y_i \equiv n_i(B)/n_i(0)$ as a function of n/n_0 . The oscillatory tendencies in the figures can be attributed to the occupation of the Landau levels by the charged particles. The oscillations become more prominent near the higher end of the density range since the magnetic field increases with the density. The electrons, being the lightest particles, show more prominent oscillations in their particle fraction ratio from an earlier density. In case of muons, the early oscillations in their profile can be explained by their lower population density, and thus lower Fermi momentum, leading to a smaller number of maximum Landau levels, which makes Landau quantization more prominent. For the magnetic field profile with $\mu = 2 \times 10^{31} Am^2$, near the surface and outer core where density is less than $2n_0$, the field strength is of the order of 10^{16} G. At this field strength the protons are not affected substantially and electrons are little affected by the presence of magnetic field, as can be seen from Fig. 5. Hence the particle fraction and threshold of Δ^- are also least affected. The proton population is affected very little and electrons populate a less number of Landau levels when the field strength reaches a magnitude of the order 10^{17} G near density $\sim 5n_0$. Then the electron fraction is increased leading to a later appearance of K^- and $\delta Y_i < 1$ for K^- in the subsequent densities. Consequently, the threshold densities of Δ^+ , Ξ^0 and Δ^{++} change and their populations are affected due to the interplay of baryon number conservation and charge neutrality condition, as seen from Fig. 5. The threshold densities of various particles are given in Table III. For the magnetic field profile with $\mu = 1.5 \times 10^{32} Am^2$, the pattern is similar but there are

some differences to be noted as evident from Fig. 6. The oscillations for δY_i of protons (p) and electrons (e^-) at the initial densities ($< 1n_0$) are noticeable. This is due to the low population of e^- and p , and the high magnitude of magnetic field, of the order 10^{17} G, for this profile near the surface and outer core. Here, we can also see that the e^- and p populations oscillate in unison. This is because they are the only charged particles at this density range and, thus, to maintain charge neutrality they must increase or decrease similarly. Similar to the case for $\mu = 2 \times 10^{31} Am^2$, the electron population increases substantially when the field strength reaches around 10^{18} G near density $3n_0$. This results in the later appearance of K^- and $\delta Y_{K^-} < 1$. The amplitudes of the oscillations in δY_{e^-} being larger compared to the case of field profile with $\mu = 2 \times 10^{31} Am^2$, the threshold density for appearance of K^- is pushed towards an even higher density in this case and δY_{K^-} is also smaller in this case. The oscillations of the charged particles are, in general, significantly larger in Fig. 6 than in Fig. 5, as expected. Similar to the case for field profile with $\mu = 2 \times 10^{31} Am^2$, the threshold densities and the particle populations for Δ^+ , Ξ^0 and Δ^{++} are also altered in the case for field profile with $\mu = 1.5 \times 10^{32} Am^2$ but the change is greater for the latter case, as can be seen from Table III. We also notice that δY_{Ξ^0} for DD-ME2 parametrization does not appear in Fig. 6 as it is very low and outside the range of the plot. This is due to its appearance being delayed because of the presence of a strong magnetic field.

In Fig. 7, we illustrate the relationship of the Dirac effective mass for nucleons as a function of n/n_0 . We

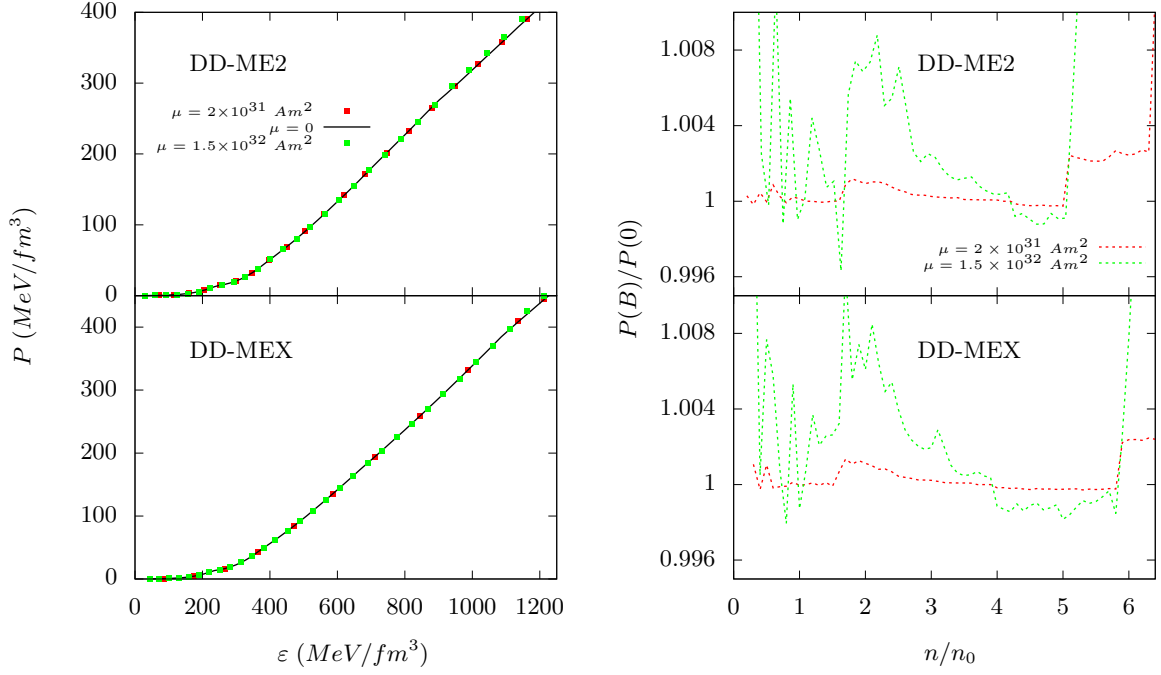


FIG. 8: Left panel: EoS for NS matter in the presence of magnetic fields with $\mu = 1.5 \times 10^{32} \text{ Am}^2$ and $\mu = 2 \times 10^{31} \text{ Am}^2$, and also for NS matter in the absence of magnetic field ($\mu = 0$). Right panel: Ratio of pressure density in the presence of the same two magnetic fields, $P(B)$, to pressure density in the absence of magnetic field, $P(0)$, as a function of the total number density normalized to n_0 (n/n_0). The plots are given for DD-ME2 (upper plots) and DD-MEX (lower plots) parametrizations. The matter composition considered is $N\bar{K}Y\Delta$.

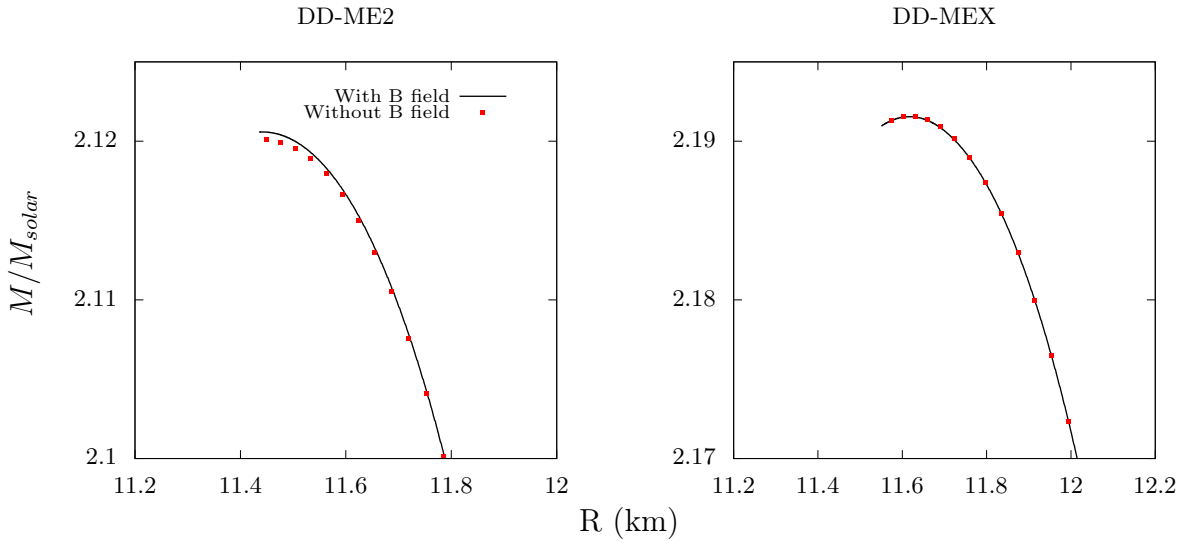


FIG. 9: Comparison of the closeup of the M-R relations in the region of the maximum mass. The plots are given for NS matter with magnetic field ($\mu = 2 \times 10^{31} \text{ Am}^2$) and without magnetic field, and for the two parametrizations: DD-ME2 (left panel) and DD-MEX (right panel). The matter composition considered is $N\bar{K}Y\Delta$.

observe that deviative features start appearing in the figures with the onset of Δ^- around density $\sim 1.6n_0$.

As a result, in the higher density regime the matter EOS stiffens. Although it is not evident from the left panel of Fig. 8 which illustrates the EOS for $N\bar{K}Y\Delta$ composition for the two parametrizations (DD-ME2 and DD-MEX) and for the two magnetic field profiles (with $\mu = 2 \times 10^{31} Am^2$ and $\mu = 1.5 \times 10^{32} Am^2$). However, the feature is evident from the right panel of Fig. 8 which shows the ratio of pressure density in presence of magnetic field $P(B)$, to pressure density without magnetic field, $P(0)$, as a function of total number density fraction, n/n_0 . The oscillations in this figure, as in the case of Fig. 5 and Fig. 6, can be attributed to the occupation of the Landau levels by the charged particles at high value of magnetic field.

Now, so far inferred maximum limit of surface magnetic field strength from the magnetar observations is of the order of $\sim 10^{16}$ G. So we consider the field profile with $\mu = 2 \times 10^{31} Am^2$ which gives the surface field strength $\sim 10^{16}$ G. With this profile the maximum field strength within the star remains below the order of 10^{17} G. Hence, for this field profile, the solution of TOV equations for the star structure can be taken as a good approximation. We show the effect of the magnetic field on the maximum mass of NS with $N\bar{K}Y\Delta$ composition in Fig. 9. We observe a small increase ($\sim 0.05\%$) in maximum mass which is visible for the case of DD-ME2 parametrization. This is the consequence of the stiffening of matter in presence of magnetic field due to late appearance of K^- .

IV. SUMMARY AND CONCLUSION

Recent observations of massive NSs [3–7] suggest the existence of matter at densities above $2n_0$ inside the core of the massive stars. At such high densities it is quite possible for exotic degrees of matter to appear. In this sce-

nario, the possibility of appearance of strange and non-strange heavier baryons, and kaons inside the core of the NSs, and its consequences on the NS observables, are of great interest and are discussed in many literature [8–19]. The effect of strong magnetic field on highly dense matter with kaons and in absence of heavier baryons has been discussed previously [26, 27]. In our present work, we discussed the effect of presence of strong magnetic field on highly dense NS matter with all possible exotic degrees of freedom, viz. hyperons, Δ -resonances and (anti)kaon condensates, in view of the existence of magnetars with high surface magnetic field. The inferred surface field strength from the magnetar observations is in the range 10^{13-16} G. The field strength inside the NSs can not be inferred from any observation as of yet but can be estimated theoretically from the solution of combined Einstein-Maxwell field equations. Hence, we considered a model magnetic field profile, as a function of baryon chemical potential inside the NS, which is poloidal in nature and satisfies the Einstein-Maxwell field equations. With this profile, the field strength gradually increases towards the centre of the star and at the centre the strength is ~ 1 order higher compared to that at the surface.

For our discussion, we considered the model of matter within DD-RMF model with two parametrizations, DD-ME2 and DD-MEX, which are compatible with the astrophysical observations for NSs, with matter composed of $N\bar{K}Y\Delta$. The variation of magnetic field with the matter density is more or less the same with these two parametrizations for the considered field profile. The presence of magnetic field pushes the threshold for appearance of K^- to a higher density. Consequently, at higher density regime, the matter stiffens compared to the case without magnetic field and this effect is more in the case of DD-ME2 parametrization than the DD-MEX parametrization. This leads to increase in the maximum attainable mass, compared to the case without magnetic field, which is also more prominent for the DD-ME2 parametrization.

-
- [1] N. K. Glendenning, *Compact stars: Nuclear physics, particle physics and general relativity* (Springer Science & Business Media, 2012).
- [2] F. Weber, R. Negreiros, P. Rosenfield, and M. Stejner, Pulsars as astrophysical laboratories for nuclear and particle physics, *Progress in Particle and Nuclear Physics* **59**, 94 (2007), international Workshop on Nuclear Physics 28th Course.
- [3] F. Özel, D. Psaltis, S. Ransom, P. Demorest, and M. Alford, THE MASSIVE PULSAR PSR j1614–2230: LINKING QUANTUM CHROMODYNAMICS, GAMMA-RAY BURSTS, AND GRAVITATIONAL WAVE ASTRONOMY, *The Astrophysical Journal* **724**, L199 (2010).
- [4] P. B. Demorest, T. Pennucci, S. M. Ransom, M. S. E. Roberts, and J. W. T. Hessels, A two-solar-mass neutron star measured using Shapiro delay, *Nature (London)* **467**, 1081 (2010), [arXiv:1010.5788 \[astro-ph.HE\]](https://arxiv.org/abs/1010.5788).
- [5] H. T. Cromartie, E. Fonseca, S. M. Ransom, P. B. Demorest, Z. Arzoumanian, H. Blumer, P. R. Brook, M. E. DeCesar, T. Dolch, J. A. Ellis, R. D. Ferdman, E. C. Ferrara, N. Garver-Daniels, P. A. Gentile, M. L. Jones, M. T. Lam, D. R. Lorimer, R. S. Lynch, M. A. McLaughlin, C. Ng, D. J. Nice, T. T. Pennucci, R. Spiewak, I. H. Stairs, K. Stovall, J. K. Swiggum, and W. W. Zhu, Relativistic Shapiro delay measurements of an extremely massive millisecond pulsar, *Nature Astronomy* **4**, 72 (2020), [arXiv:1904.06759 \[astro-ph.HE\]](https://arxiv.org/abs/1904.06759).
- [6] J. Antoniadis, P. C. C. Freire, N. Wex, T. M. Tauris, R. S. Lynch, M. H. van Kerkwijk, M. Kramer, C. Bassa, V. S. Dhillon, T. Driebe, J. W. T. Hessels,

- V. M. Kaspi, V. I. Kondratiev, N. Langer, T. R. Marsh, M. A. McLaughlin, T. T. Pennucci, S. M. Ransom, I. H. Stairs, J. van Leeuwen, J. P. W. Verbiest, and D. G. Whelan, A Massive Pulsar in a Compact Relativistic Binary, *Science* **340**, 448 (2013), [arXiv:1304.6875 \[astro-ph.HE\]](#).
- [7] R. W. Romani, D. Kandel, A. V. Filippenko, T. G. Brink, and W. Zheng, PSR j0952-0607: The fastest and heaviest known galactic neutron star, *The Astrophysical Journal Letters* **934**, L17 (2022).
- [8] V. A. Ambartsumyan and G. S. Saakyan, The Degenerate Superdense Gas of Elementary Particles, *Sov. Astron.* **4**, 187 (1960).
- [9] J. J. Li, A. Sedrakian, and F. Weber, Competition between delta isobars and hyperons and properties of compact stars, *Physics Letters B* **783**, 234 (2018).
- [10] J. J. Li and A. Sedrakian, Implications from GW170817 for Δ -isobar admixed hypernuclear compact stars, *The Astrophysical Journal* **874**, L22 (2019).
- [11] A. Drago, A. Lavagno, and G. Pagliara, Can very compact and very massive neutron stars both exist?, *Phys. Rev. D* **89**, 043014 (2014).
- [12] P. Char and S. Banik, Massive neutron stars with antikaon condensates in a density-dependent hadron field theory, *Phys. Rev. C* **90**, 015801 (2014).
- [13] N. K. Glendenning and J. Schaffner-Bielich, First order kaon condensate, *Phys. Rev. C* **60**, 025803 (1999).
- [14] S. Banik and D. Bandyopadhyay, Antikaon condensation and the metastability of protoneutron stars, *Phys. Rev. C* **63**, 035802 (2001).
- [15] M. Prakash, I. Bombaci, M. Prakash, P. J. Ellis, J. M. Lattimer, and R. Knorren, Composition and structure of protoneutron stars, *Physics Reports* **280**, 1 (1997).
- [16] J. Schaffner and I. N. Mishustin, Hyperon-rich matter in neutron stars, *Phys. Rev. C* **53**, 1416 (1996).
- [17] S. Banik and D. Bandyopadhyay, Third family of superdense stars in the presence of antikaon condensates, *Phys. Rev. C* **64**, 055805 (2001).
- [18] T. Malik, S. Banik, and D. Bandyopadhyay, New equation of state involving bose-einstein condensate of antikaon for supernova and neutron star merger simulations, *European Physical Journal-special Topics* , 1 (2021).
- [19] V. B. Thapa and M. Sinha, Dense matter equation of state of a massive neutron star with antikaon condensation, *Phys. Rev. D* **102**, 123007 (2020).
- [20] M. C. Miller, F. K. Lamb, A. J. Dittmann, S. Bogdanov, Z. Arzoumanian, K. C. Gendreau, S. Guillot, A. K. Harding, W. C. G. Ho, J. M. Lattimer, R. M. Ludlam, S. Mahmoodifar, S. M. Morsink, P. S. Ray, T. E. Strohmayer, K. S. Wood, T. Enoto, R. Foster, T. Okajima, G. Prigozhin, and Y. Soong, PSR j0030+0451 mass and radius from nicer data and implications for the properties of neutron star matter, *The Astrophysical Journal* **887**, L24 (2019).
- [21] T. E. Riley, A. L. Watts, S. Bogdanov, P. S. Ray, R. M. Ludlam, S. Guillot, Z. Arzoumanian, C. L. Baker, A. V. Bilous, D. Chakrabarty, K. C. Gendreau, A. K. Harding, W. C. G. Ho, J. M. Lattimer, S. M. Morsink, and T. E. Strohmayer, A nicer view of PSR j0030+0451: Millisecond pulsar parameter estimation, *The Astrophysical Journal* **887**, L21 (2019).
- [22] A. K. Harding and D. Lai, Physics of strongly magnetized neutron stars, *Reports on Progress in Physics* **69**, 2631 (2006).
- [23] R. Turolla, S. Zane, and A. L. Watts, Magnetars: the physics behind observations. a review, *Reports on Progress in Physics* **78**, 116901 (2015).
- [24] V. B. Thapa, M. Sinha, J. J. Li, and A. Sedrakian, Massive Δ -resonance admixed hypernuclear stars with antikaon condensations, *Phys. Rev. D* **103**, 063004 (2021).
- [25] V. B. Thapa, M. Sinha, J. J. Li, and A. Sedrakian, Equation of state of strongly magnetized matter with hyperons and Δ -resonances, *Particles* **3**, 660 (2020).
- [26] P. Yue and H. Shen, Quark-meson coupling model for antikaon condensation in neutron star matter with strong magnetic fields, *Phys. Rev. C* **77**, 045804 (2008).
- [27] M. Kumari and A. Kumar, Antikaon condensation in magnetized neutron stars, *International Journal of Modern Physics E* **31**, 2250050 (2022).
- [28] S. Pal, D. Bandyopadhyay, and W. Greiner, Antikaon condensation in neutron stars, *Nuclear Physics A* **674**, 553 (2000).
- [29] A. Broderick, M. Prakash, and J. M. Lattimer, The equation of state of neutron star matter in strong magnetic fields, *The Astrophysical Journal* **537**, 351 (2000).
- [30] A. Rabhi, M. A. Pérez-García, C. Providência, and I. Vidaña, Magnetic susceptibility and magnetization properties of asymmetric nuclear matter in a strong magnetic field, *Phys. Rev. C* **91**, 045803 (2015).
- [31] R. H. Casali, L. B. Castro, and D. P. Menezes, Hadronic and hybrid stars subject to density-dependent magnetic fields, *Phys. Rev. C* **89**, 015805 (2014).
- [32] R. L. Bowers and E. P. T. Liang, Anisotropic Spheres in General Relativity, *Astrophys. J.* **188**, 657 (1974).
- [33] D. Chatterjee, J. Novak, and M. Oertel, Magnetic field distribution in magnetars, *Phys. Rev. C* **99**, 055811 (2019).
- [34] D. Chatterjee, T. Elghozi, J. Novak, and M. Oertel, Consistent neutron star models with magnetic-field-dependent equations of state, *Monthly Notices of the Royal Astronomical Society* **447**, 3785 (2015) <https://academic.oup.com/mnras/article-pdf/447/4/3785/5792844/s>
- [35] V. Dexheimer, B. Franzon, and S. Schramm, A self-consistent study of magnetic field effects on hybrid stars, *Journal of Physics: Conference Series* **861**, 012012 (2017).
- [36] F. Hofmann, C. M. Keil, and H. Lenske, Application of the density dependent hadron field theory to neutron star matter, *Phys. Rev. C* **64**, 025804 (2001).
- [37] J. J. Li and A. Sedrakian, Constraining compact star properties with nuclear saturation parameters, *Phys. Rev. C* **100**, 015809 (2019).
- [38] T. Waas and W. Weise, S-wave interactions of \bar{K} and η mesons in nuclear matter, *Nuclear Physics A* **625**, 287 (1997).
- [39] E. Friedman, A. Gal, J. Mareš, and A. Cieplý, K^- -nucleus relativistic mean field potentials consistent with kaonic atoms, *Phys. Rev. C* **60**, 024314 (1999).
- [40] V. Koch, K^- -proton scattering and the $\Lambda(1405)$ in dense matter, *Physics Letters B* **337**, 7 (1994).
- [41] M. Lutz, Nuclear kaon dynamics, *Physics Letters B* **426**, 12 (1998).
- [42] J. Schaffner-Bielich, V. Koch, and M. Effenberger, Medium modified cross sections, temperature and finite momentum effects for antikaon production in heavy-ion collisions, *Nuclear Physics A* **669**, 153 (2000).
- [43] N. Gupta and P. Arumugam, Neutron stars with antikaons: Comparison between two ways of extending the relativistic mean field models,

- Phys. Rev. C* **87**, 045802 (2013).
- [44] G. A. Lalazissis, T. Nikšić, D. Vretenar, and P. Ring, New relativistic mean-field interaction with density-dependent meson-nucleon couplings, *Phys. Rev. C* **71**, 024312 (2005).
- [45] S. Typel, G. Röpke, T. Klähn, D. Blaschke, and H. H. Wolter, Composition and thermodynamics of nuclear matter with light clusters, *Phys. Rev. C* **81**, 015803 (2010).
- [46] A. Taninah, S. Agbemava, A. Afanasjev, and P. Ring, Parametric correlations in energy density functionals, *Physics Letters B* **800**, 135065 (2020).
- [47] T. E. Riley, A. L. Watts, P. S. Ray, S. Bogdanov, S. Guillot, S. M. Morsink, A. V. Bilous, Z. Arzoumanian, D. Choudhury, J. S. Deneva, K. C. Gendreau, A. K. Harding, W. C. G. Ho, J. M. Lattimer, M. Loewenstein, R. M. Ludlam, C. B. Markwardt, T. Okajima, C. Prescod-Weinstein, R. A. Remillard, M. T. Wolff, E. Fonseca, H. T. Cromartie, M. Kerr, T. T. Pennucci, A. Parthasarathy, S. Ransom, I. Stairs, L. Guillemot, and I. Cognard, A NICER View of the Massive Pulsar PSR J0740+6620 Informed by Radio Timing and XMM-Newton Spectroscopy, *Astro. Phys. J. Lett.* **918**, L27 (2021), [arXiv:2105.06980](https://arxiv.org/abs/2105.06980) [astro-ph.HE].
- [48] M. C. Miller, F. K. Lamb, A. J. Dittmann, S. Bogdanov, Z. Arzoumanian, K. C. Gendreau, S. Guillot, W. C. G. Ho, J. M. Lattimer, M. Loewenstein, S. M. Morsink, P. S. Ray, M. T. Wolff, C. L. Baker, T. Cazeau, S. Manthripragada, C. B. Markwardt, T. Okajima, S. Pollard, I. Cognard, H. T. Cromartie, E. Fonseca, L. Guillemot, M. Kerr, A. Parthasarathy, T. T. Pennucci, S. Ransom, and I. Stairs, The Radius of PSR J0740+6620 from NICER and XMM-Newton Data, *Astro. Phys. J. Lett.* **918**, L28 (2021), [arXiv:2105.06979](https://arxiv.org/abs/2105.06979) [astro-ph.HE].
- [49] R. W. Romani, D. Kandel, A. V. Filippenko, T. G. Brink, and W. Zheng, PSR J1810+1744: Companion Darkening and a Precise High Neutron Star Mass, *Astro. Phys. J. Lett.* **908**, L46 (2021), [arXiv:2101.09822](https://arxiv.org/abs/2101.09822) [astro-ph.HE].
- [50] M. C. Miller, F. K. Lamb, A. J. Dittmann, S. Bogdanov, Z. Arzoumanian, K. C. Gendreau, S. Guillot, A. K. Harding, W. C. G. Ho, J. M. Lattimer, R. M. Ludlam, S. Mahmoodifar, S. M. Morsink, P. S. Ray, T. E. Strohmayer, K. S. Wood, T. Enoto, R. Foster, T. Okajima, G. Prigozhin, and Y. Soong, PSR J0030+0451 Mass and Radius from NICER Data and Implications for the Properties of Neutron Star Matter, *Astro. Phys. J. Lett.* **887**, L24 (2019), [arXiv:1912.05705](https://arxiv.org/abs/1912.05705) [astro-ph.HE].
- [51] T. E. Riley, A. L. Watts, S. Bogdanov, P. S. Ray, R. M. Ludlam, S. Guillot, Z. Arzoumanian, C. L. Baker, A. V. Bilous, D. Chakrabarty, K. C. Gendreau, A. K. Harding, W. C. G. Ho, J. M. Lattimer, S. M. Morsink, and T. E. Strohmayer, A NICER View of PSR J0030+0451: Millisecond Pulsar Parameter Estimation, *Astro. Phys. J. Lett.* **887**, L21 (2019), [arXiv:1912.05702](https://arxiv.org/abs/1912.05702) [astro-ph.HE].
- [52] J.-L. Jiang, S.-P. Tang, Y.-Z. Wang, Y.-Z. Fan, and D.-M. Wei, PSR j0030+0451, GW170817, and the nuclear data: Joint constraints on equation of state and bulk properties of neutron stars, *The Astrophysical Journal* **892**, 55 (2020).
- [53] P. Landry, R. Essick, and K. Chatziioannou, Non-parametric constraints on neutron star matter with existing and upcoming gravitational wave and pulsar observations, *Phys. Rev. D* **101**, 123007 (2020), [arXiv:2003.04880](https://arxiv.org/abs/2003.04880) [astro-ph.HE].
- [54] B. P. Abbott, R. Abbott, *et al.*, GW170817: Observation of Gravitational Waves from a Binary Neutron Star Inspiral, *Phys. Rev. Lett.* **119**, 161101 (2017), [arXiv:1710.05832](https://arxiv.org/abs/1710.05832) [gr-qc].
- [55] B. P. Abbott, R. Abbott, *et al.* (LIGO Scientific Collaboration and Virgo Collaboration), Properties of the binary neutron star merger gw170817, *Phys. Rev. X* **9**, 011001 (2019).
- [56] V. Dexheimer, B. Franzon, R. Gomes, R. Farias, S. Avancini, and S. Schramm, What is the magnetic field distribution for the equation of state of magnetized neutron stars?, *Physics Letters B* **773**, 487 (2017).
- [57] I. A. Rather, U. Rahaman, V. Dexheimer, A. Usmani, and S. Patra, Heavy magnetic neutron stars, *arXiv preprint arXiv:2104.05950* (2021).